International Journal of Pharmaceutics 465 (2014) 143–158

Contents lists available at ScienceDirect

International Journal of Pharmaceutics

journal homepage: www.elsevier.com/locate/ijpharm

Enhancing the intestinal absorption of low molecular weight chondroitin sulfate by conjugation with α-linolenic acid and the transport mechanism of the conjugates

Yuliang Xiao [a,b], Pingli Li [a], Yanna Cheng [c], Xinke Zhang [a], Juzheng Sheng [a], Decai Wang [b], Juan Li [a], Qian Zhang [a], Chuanqing Zhong [a], Rui Cao [a], Fengshan Wang [a,d,*]

[a] Key Laboratory of Chemical Biology of Natural Products (Ministry of Education), Institute of Biochemical and Biotechnological Drugs, School of Pharmaceutical Sciences, Shandong University, Jinan 250012, China
[b] College of Pharmaceutical Sciences, Taishan Medical University, Taian 271000, China
[c] Department of Pharmacology, School of Pharmaceutical Sciences, Shandong University, Jinan 250012, China
[d] National Glycoengineering Research Center, Shandong University, Jinan 250012, China

ARTICLE INFO

Article history:
Received 31 October 2013
Received in revised form 13 January 2014
Accepted 7 February 2014
Available online 10 February 2014

Keywords:
Chondroitin sulfate
α-Linolenic acid
Transport mechanism
Oral delivery
Self-aggregates

ABSTRACT

The purpose of this report was to demonstrate the effect of amphiphilic polysaccharides-based self-assembling micelles on enhancing the oral absorption of low molecular weight chondroitin sulfate (LMCS) *in vitro* and *in vivo*, and identify the transepithelial transport mechanism of LMCS micelles across the intestinal barrier. α-Linolenic acid-low molecular weight chondroitin sulfate polymers(α-LNA–LMCS) were successfully synthesized, and characterized by FTIR, ^{1}HNMR, TGA/DSC, TEM, laser light scattering and zeta potential. The significant oral absorption enhancement and elimination half-life ($t_{1/2}$) extension of LNA–LMCS2 in rats were evidenced by intragastric administration in comparison with CS and LMCS. Caco-2 transport studies demonstrated that the apparent permeability coefficient (P_{app}) of LNA–LMCS2 was significantly higher than that of CS and LMCS ($p < 0.001$), and no significant effects on the overall integrity of the monolayer were observed during the transport process. In addition, α-LNA–LMCS micelles accumulated around the cell membrane and intercellular space observed by confocal laser scanning microscope (CLSM). Furthermore, evident alterations in the F-actin cytoskeleton were detected by CLSM observation following the treatment of the cell monolayers with α-LNA–LMCS micelles, which further certified the capacity of α-LNA–LMCS micelles to open the intercellular tight junctions rather than disrupt the overall integrity of the monolayer. Therefore, LNA–LMCS2 with low cytotoxicity and high bioavailability might be a promising substitute for CS in clinical use, such as treating osteoarthritis, atherosclerosis, etc.

1. Introduction

Chondroitin sulfate (CS) ubiquitously distributes on cell surfaces and in the extracellular matrix (ECM) of mammalian animals. CS is particularly abundant in bones, tendons, blood vessels, nerve tissues, and cartilage (Deepa et al., 2007). CS, a sulfated glycosaminoglycan (GAG), is composed of a repeating disaccharide unit of glucuronic acid (GlcA) and *N*-acetylgalactosamine (GalNAc), which is commonly sulfated at the C-4 and/or C-6 of GalNAc in mammals (Sugahara et al., 2003). CS has been discovered to have various biological functions including anti-oxidation (Muller et al., 2010), anti-inflammation (Cervigni et al., 2012; Gabay et al., 2011; Reginster, 2012), anti-atherosclerosis (Delgado-Roche et al., 2013), immunoregulation (Moller et al., 2010; Sakai et al., 2006), regulating cell adhesion and morphogenesis (Mizuguchi et al., 2003; Nandini and Sugahara, 2006). In addition, CS also plays important roles in central nervous system development (Sugahara and Mikami, 2007) and signal transduction (Sato et al., 2008). The market for products containing CS and glucosamine is developing in North America, Europe, South East Asia and Australia. In United States, CS is recognized as a "dietary supplement". And while in Europe, CS is marketed as symptomatic slow-acting drugs for osteoarthritis and is widely used for the relief of symptoms and pain of arthritic diseases.

* Corresponding author at: Institute of Biochemical and Biotechnologica Drugs, School of Pharmaceutical Sciences, Jinan 250012, Shandong, China. Tel.: +86 531 88382589; fax: +86 531 88382548.
E-mail addresses: 111925wj@163.com, fswang@sdu.edu.cn (F. Wang).

http://dx.doi.org/10.1016/j.ijpharm.2014.02.009
0378-5173/

The main problem affecting the efficacy CS is its poor intestinal absorption, resulting from its high molecular weight, charge density, as well as hydrophilicity (Baici et al., 1992). Therefore, intestinal absorption became one of critical factors for the successful application of CS and CS derivatives in the treatment of osteoarthritis and atherosclerosis. Some results reported in recent years have demonstrated that oral delivery systems, including amphiphilic polysaccharides, liposomes, enteric coatings, and the addition of absorption enhancers, could be possible ways to improve the oral absorption of polysaccharides (Kim et al., 2006; Mo et al., 2011; Qian et al., 2013; Salartash et al., 2000). Drug carriers can be employed to target transport carrier proteins or to open tight junctions between the epithelial cells, so as to facilitate the absorption of polysaccharides. Nano-sized polymeric micelles have been successfully applied in oral drug delivery system. The core-shell structure of such self-assembling systems presents advantages besides the improvement of drug absorption, such as lower cytotoxicity, higher solubility, and good stability(Yao et al., 2011; Zhang et al., 2010). What is more, almost all of the nano-sized polymeric micelles of polysaccharides are documented to be chitosan, heparin, pullulan (Duhem et al., 2012; Kim et al., 2006; Mo et al., 2011; Salartash et al., 2000). However, few works have focused on the use of self-assembling micelles as the drug carrier systems for oral administration of CS. Here, we want to figure out whether low molecular weight amphiphilic polysaccharides-based self-assembling micelles would enhance the oral absorption of CS. Esterification is considered as a method to improve the hydrophobicity for many polysaccharides. α-Linolenic acid (α-LNA) is an essential fatty acid that cannot be synthesized in humans body but only obtained from the diet. α-LNA can be converted into eicosapentaenoic acid (EPA) and docosahexaenoic acid (DHA) in the body, although conversion only occurs to a limited extent(Brenna et al., 2009; Burdge and Calder, 2006). Apart from potential indirect effects on cardiovascular diseases via conversion into EPA and DHA, α-LNA also has direct anti-inflammatory (Stark et al., 2008), antiarrhythmic (Albert et al., 2005), anti-thrombotic (Campos et al., 2008) and neuroprotective effects (Nguemeni et al., 2010). Therefore, the modification of low molecular weight chondroitin sulfate (LMCS) with α-LNA may improve the hydrophobicity of LMCS, thereby leading to a positive synergistic effect on anti-inflammation and anti-atherosclerosis.

In this work, we prepared LMCS micelles using α-LNA as the hydrophobic chain of the micelle-forming materials. The physicochemical characteristics of α-LNA–LMCSs were investigated by FTIR, ^{1}HNMR, TGA/DSC, TEM, laser light scattering and zeta potential. The oral bioavailability of α-LNA–LMCS micelles *in vivo* was evaluated by determining the α-LNA–LMCS concentrations in plasma levels following oral administration to rats in comparison with CS, and Caco-2 cell monolayers representing *in vitro* model of the intestinal epithelial barrier were used to determine the intestinal transport ability of α-LNA–LMCS micelles. All these results indicated that the α-LNA–LMCS micelles could enhance the intestinal absorption of CS. Furthermore, we used confocal laser scanning microscope (CLSM) to study the possible mechanisms, and found that the enhancement of absorption was depending on the paracellular pathway and endocytosis.

2. Materials and methods

2.1. Materials and animals

The average molecular weights of chondroitin sulfate (CS) (Huamao Shuanghui Co., Ltd., Luohe, China) and Low molecular weight chondroitin sulfate (LMCS, prepared in our lab) were 17.5 kDa and 4.1 kDa, respectively. The LMCS was obtained by chemical depolymerization with hydrogen peroxide. Chondroitin sulfate sodium salt from bovine cartilage, 3-(4,5-dimethylthiazol-2-yl)-2,5-diphenyltetrazolium bromide (MTT), dimethyl sulfoxide (DMSO) and 1,9-dimethyl- methylene blue (DMMB) were obtained from Sigma–Aldrich (St. Louis, MO, USA). α-Linolenic acid, 5-aminofluorescein (5-AMF), 1-ethyl-(dimethylaminopropyl) carbodiimide (EDC), 4-Dimethylaminopyridine(DMAP), Hoechst 33342 and pyrene were purchased from Aladdin Chemistry Co., Ltd. (Shanghai, China). Dialysis membranes (MWCO 1000), Tris (hydroxymethyl) aminomethane (Tris), Triton X-100 and phenol (saturated with water) were obtained from the Shanghai Medical Chemical Reagent Co., Ltd. (Shanghai, China). Dulbecco's Modified Eagle Medium (DMEM), Fetal bovine serum (FBS), 0.25% trypsine and Hanks balance salt solution (HBSS) were purchased from Gibco, Invitrogen Corp (Ontario, USA). Confocal dishes, 25 cm^2 plastic culture flasks, 6-well and 96-well tissue culture plates were obtained from Costar (Corning Incorporated, USA). Millicell 6-well plate (12 mm, 3.0 mm pore size inserts) and actinase E were purchased from Merck Millipore (Shanghai, China). Rhodamin-phalloidin was purchased from Biotium, Inc. (Hayward, USA). 1′-dioctadecyl-3,3,3′,3′-tetramethylindocarbocyanine perchlorate (DiI) was purchased Beyotime Institute of Biotechnology (Jiangsu, China). All the other chemicals and reagents used were of analytical purity grade or higher, obtained commercially.

Clean grade Sprague–Dawley rats weighing 230 ± 10 g were obtained from Beijing HFK Bioscience Co., LTD (China, Document No. SCXK 2009-0004). Rats were housed under 12 h light/dark cycle conditions, with food and water freely available. Temperature and relative humidity were maintained at 25 ± 1 °C and (55 ± 5%), respectively. All care and handling of animals were performed with the approval of the Institutional Animal Care and Use Committee of Shandong University. Guidelines of Institutional Animal Ethics Committee were followed for *in vivo* experiments.

2.2. Synthesis of α-linolenic acid-low molecular weight chondroitin sulfate polymers

α-LNA–LMCS was synthesized by the method as follows: 1 mmol of LMCS and 0.1 g of DMAP were dissolved in 10 mL of formamide by vigorous stirring at 55 °C. To this solution, 0.1, 0.5, 1, or 2 mmol of α-linoleoyl chloride were added to change the esterification degree. The mixture was stirred at 55 °C for 1 h. The product was dialyzed using dialysis membrane (MWCO 1000) in deionized water for two days to remove excess reagents and formamide, and further dialyzed against 95% ethanol for two days to remove unconjugated α-linolenic acid. A yellowish precipitate was thus obtained and purified by precipitation with 50 mL of 95% ethanol. The solid material was vacuum-dried for 24 h, and a yellowish powder was obtained. The resulting products were designated as LNA–LMCS1, LNA–LMCS2, LNA–LMCS3 and LNA–LMCS4, respectively. The synthetic procedure of α-LNALMCS polymers was shown in Fig. 1.

2.3. Preparation of α-LNA–LMCS micelles

α-LNA–LMCS micelles were prepared via dialysis (Yang et al., 2009) α-LNA–LMCS(5 mg) was dissolved in 3 mL of formamide. To form the nanomicelles, the prepared solution was dialyzed using MWCO 1000 membrane in deionised water. After two days, the dialysates were collected and diluted to 10 mL with water (final concentration 0.5 mg/mL). The solution of α-LNA–LMCS micelles was stored at 4 °C. The total preparation process was shown in Fig. 2.

2.4. Physicochemical characterization of CS and its derivatives

2.4.1. Recording of Fourier transform infrared spectra

Fourier transform infrared (FTIR) spectra were recorded with a NEXUS 470 spectrometer (Nicolet, USA) by KBr method.

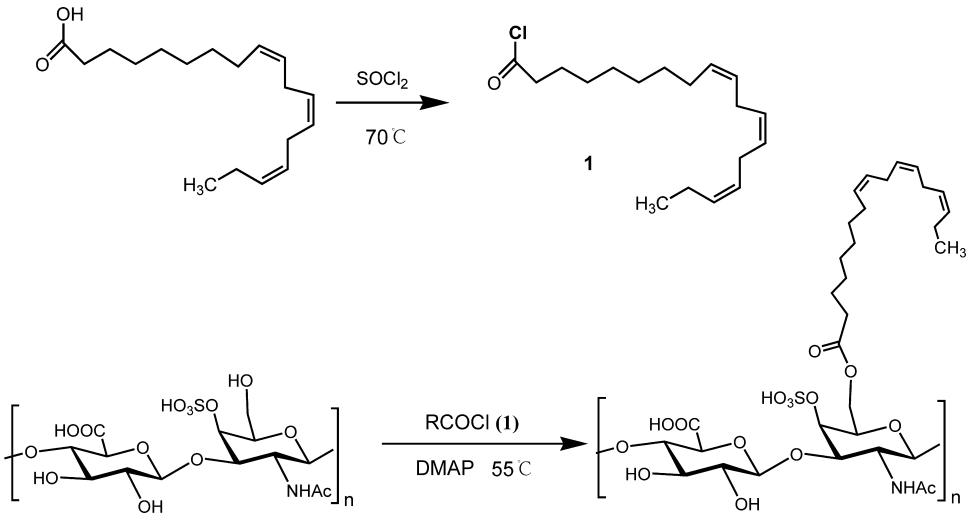

Fig. 1. Reaction scheme for the synthesis of α-LNA–LMCS.

2.4.2. ^{1}HNMR measurement

^{1}HNMR spectra were recorded with a AVANCE 600 spectrometer at 600 MHz, using tetramethylsilane (TMS) as an internal standard. The degree of substitution for the derivatives of CS were evaluated by ^{1}HNMR.

2.4.3. Thermal analysis

The thermal gravimetry analysis and differential scanning calorimetry (TGA/DSC) measurement were carried out from 30 to 400 °C using a TGA/DSC1-1600HT instrument under air flux, at a heating rate of 10 °C/min. Samples were weighed on a platinum crucible with a microprocessor-driven temperature-control unit and a data station.

2.4.4. Dynamic light scattering and zeta potential measurements

Size and the size distribution of the prepared micelles were measured by the dynamic laser light scattering gonimeter (BI-9000, Brookhaven, USA). The polydispersity index ranged from 0 to 1. The zeta potential of micelles was determined by photon correlation spectroscopy (PCS) with a Zetasizer 3000 (Malvern Instruments, Malvern, UK). The concentration of micelles was kept constant at 1.0 mg/mL. The average particle size was expressed as volume mean diameter and the reported value was represented as mean ± SD ($n = 3$).

2.4.5. Morphology observation of α-LNA–LMCS micelles

The morphology and size of α-LNA–LMCS micelles were observed using a transmission electron microscope (TEM). A drop of sample solution (1 mg/mL) was placed onto a 300-mesh copper grid coated with carbon. After 1 min, the grid was tapped with a filter paper to remove surface water, followed by air drying and negatively stained with 2% phosphotungstic acid for 30 s. The grid was dried at room temperature and observations were performed at 80 kV.

2.4.6. Critical aggregation concentration of self-aggregated micelles

The critical aggregation concentration (CAC) of the α-LNALMCS micelles were estimated by the probe fluorescence technique (Mi et al., 2011), using pyrene as the fluorescence probe. A pyrene stock solution (6.0×10^{-3} mol/L) was prepared in acetone and stored at 4 °C. For the measurement of steady-state fluorescence spectra, a certain amount of pyrene solutions (3×10^{-4} mol/L) in acetone were added to a series of vials, followed by evaporation to remove the acetone. Then, the acetone-free pyrene was mixed with solutions of α-LNA–LMCSs, and the concentrations of which ranged from 1×10^{-4} to 0.5 mg/mL. The final pyrene concentration in each sample solution was 6.0×10^{-7} mol/L. The excitation and emission slit widths were set to 5 and 2.5 nm, respectively. The emission spectra of pyrene were recorded from 350 to 500 nm using a

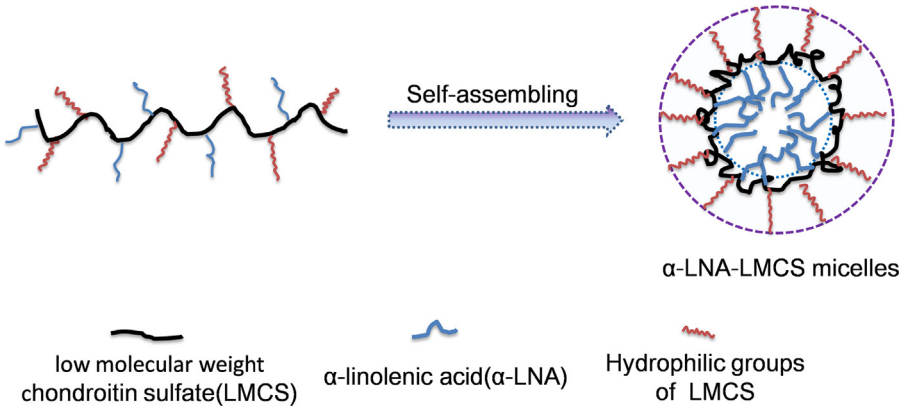

Fig. 2. The schematic representation of the formation of the self-assembled α-LNA–LMCS micelles.

fluorescence spectrophotometer (F-2500, Hitachi, Japan). The fluorescence intensity ratio of I_{372}/I_{383} was analyzed as a function of micelle concentration.

2.5. Quantitative analysis of absorbed CS in rat plasma

Hundred μL of plasma was added to 100 μL of 50 mmol/L Tris–HCl buffer (pH 8.0) containing 2% actinase E and the mixture was incubated at 50 °C for 20 h. Then, the mixture was extracted twice with 200 μL of phenol:chloroform:isoamyl alcohol (25:24:1), followed by two times extraction with 200 μL of chloroform. The CS in raffinate phase was then obtained by vacuum freeze drying. The dried CS was dissolved in 100 μL of water and the CS level in plasma was quantified by the DMMB assay (Sim et al., 2005).

2.6. In vivo *absorption efficacy assessment*

Normal male Sprague-Dawley rats were randomly divided into 6 groups (6 each) and fasted overnight but allowed access to water ad libitum prior to the experiment. Then six groups of rats were administered intragastrically with CS and its derivatives solution in PBS (pH 7.4), respectively. And the volume of CS and its derivatives given was determined by ensuring a dose of 200 mg/kg. After the oral administration, blood samples (500 μL) were taken from the capillary in the retro-orbital venous plexus at predetermined time intervals (0, 0.25, 0.5, 1, 2, 4, 8, 12 and 24 h) and immediately mixed with EDTA anticoagulant. Plasma was prepared by centrifugation at 900 × *g* for 5 min at 4 °C and stored at −80 °C until analysis.

2.7. Cell culture

The human colon adenocarcinoma cells (Caco-2) were obtained from the Institute of Nautical Medicine, Nantong University (Nantong China). The Caco-2 cells were routinely maintained in DMEM with 4.5 g/L of D-glucose, supplemented with 10% of heat inactivated FBS, 1% of nonessential amino acids, 100 U/mL of penicillin, 100 μg/mL of streptomycin and 2 mmol/L of L-glutamine. The cells were cultured in a humidified atmosphere containing 5% CO_2 at 37 °C. The cells were subcultivated every 5 days at 80–90% confluence using trypsin–EDTA at a split ratio of 1:2. The Caco-2 cells used for experiments were between passage 35 and 55.

2.8. Measurement of the transepithelial electrical resistance

Measurement of transepithelial electrical resistance(TEER) was performed to evaluate possible damage of the cellular monolayer during the experiments. The TEER of monolayers was checked using a Millicell® ERS meter (Millipore, Bedford, MA, USA). Prior to the experiment, the cells were washed twice with phosphate buffered saline (PBS) and pre-equilibrated for 1 h with HBSS at pH 7.4. After removing the medium, the Caco-2 cell monolayers were treated with CS and its derivative solutions (4, 20, 100 and 500 μg/mL in HBSS) in the apical compartment. The TEER was measured every 20 min. After 2 h of treatment, the cells were carefully washed twice with PBS and incubated with fresh culture medium. The recovery of TEER values was monitored for 24 h after the treatment.

2.9. Transport studies across Caco-2 cell monolayers

The feasibility of α-LNA–LMCS micelles for use as an oral dosage form was evaluated by determining the permeability of α-LNA–LMCS across Caco-2 cell monolayers at pH 7.4 (Qian et al., 2013). The Caco-2 cells were seeded on the permeable polycarbonate inserts in Millicell (6-well) plates at a density of approximately 5×10^4 cells/cm^2. The culture medium (2 mL per insert and 3 mL per well) was replaced every two days for the first week and everyday thereafter. After 19–21 days in culture, the TEER of monolayers was checked using a Millicell®-ER system. Caco-2 monolayers could only be used in the experiments when TEER values reached 300–600 Ω/cm^{2}and phenol red permeability was less than 0.5% per hour. Prior to the experiment, the cells were washed twice with PBS and pre-equilibrated for 30 min with HBSS at 37 °C. After removing the HBSS, 2 mL of CS and its derivatives solution (0.1 mg/mL) was added on the apical side (AP) of the monolayers while the basolateral side (BL) compartment was filled with 4 mL HBSS. Samples (400 μL) were taken at 30, 60, 90, 120, 180, 210 and 240 min from the basolateral side and replaced with equal volumes of fresh HBSS. The amount of CS and its derivatives was quantified by the DMMB assay (Sim et al., 2005). All experiments were repeated three times at 37 °C. The apparent permeability coefficient was calculated with the following Eq. (1):

$$P_{app} = \left(\frac{dQ}{dt}\right) \times \left(\frac{1}{AC_0}\right)$$

where P_{app} is the apparent permeability coefficient (cm/s), dQ/dt (μg/s) is the rate of appearance of CS and its derivatives on the basolateral side, A is the surface area of the Caco-2 cell monolayers, and C_0 (μg/mL) is the initial drug concentration.

Absorption enhancement ratios (R) were calculated from P_{app} values by using Eq. (2) (Kotze et al., 1998):

$$R = \frac{P_{app}(\text{sample})}{P_{app}(\text{control})}$$

In this study, efflux ratio was used to evaluate the function of P-gp. This ratio was calculated with the following Eq. (3):

$$\text{Efflux ratio} = \frac{P_{app(AP-BL)}}{P_{app(BL-AP)}}$$

where $P_{app(AP-BL)}$ is the intestinal apparent permeability coefficient from the apical side to the basolateral side and $P_{app(BL-AP)}$ is the intestinal apparent permeability coefficient from the basolateral side to the apical side.

2.10. Cytotoxicity studies in Caco-2 cells and HT29 cells

To investigate the biocompatibility of both CS and α-LNA–LMCS micelles, the MTT assay was used to evaluate their cytotoxicities against Caco-2 cells and HT29 cells (Mosmann, 1983). Briefly, Caco-2 cells and HT29 cells in their logarithmic growth phase were seeded in 96-well plates at a seeding density of 8000 cells/well in100 μL medium, respectively. After the cells adhered to the plates, the culture medium in each well was replaced with 150 μL of the test samples (α-LNA–LMCS solutions with final concentration ranging from 20 to 500 μg/mL in complete DMEM medium). Cells were incubated for different times (48, 72 h) and then the viability of the cells was determined using MTT assay. The absorbance of each well was measured at 570 nm with a microplate reader (Bio-Rad 680, USA). The relative cell viability was calculated with the following Eq. (4):

$$\text{Relative cell viability}\ (\%) = \frac{A_{570\ \text{Sample}} - A_{570\ \text{Blank}}}{A_{570\ \text{Control}} - A_{570\ \text{Blank}}} \times 100$$

2.11. Preparation and purification of 5-aminofluorescein-labeled chondroitin sulfate and its derivatives

Covalent binding of 5-aminofluorescein (5-AMF) to CS and its derivatives was performed according to the methods described in a previous report (Mohan et al., 2012). The CS and its derivatives (20 mg) and EDC (15 mg) were dissolved in 2 mL water (pH5.0) and

stirred for 40 min, then 2 mL of 5-AMF solution in 50% ethanol containing 2 mg of 5-AMF was added to CS or its derivertive solutions. This mixture was incubated at room temperature for overnight in darkness. After that, the product was dialyzed in deionized water using MWCO 1000 membrane for two days and further dialyzed against 50% ethanol for two days to remove excess reagents and unconjugated 5-AMF. The labeled CS and its derivatives were then separated from the dialyzed solution by gel filtration on a 1.4 cm × 60 cm column of SephadexG-10 in deionized water. After dialysis and chromatographic separation, 5-AMF-labeled CS and its derivatives were obtained by freeze-drying. Thin-layer chromatography on silica-gel, used for identification of 5-AMF-labeled CS and its derivatives, was performed using 33% isopropanol (isopropanol:H_2O = 3:1) as developing agent. All steps were carried out in darkness.

2.12. Confocal microscopy study

Caco-2 cells were seeded in confocal dishs at a density of 1×10^5 cells/3.5-cm dish and cultured for 4 days at 37 °C in 5% CO_2. After the medium was removed, the cells were washed twice with HBSS. 0.5 mL of pre-warmed fresh HBSS was added and the cells were then cultured at 37 °C for 30 min. After the medium was removed, 0.3 mL of CS and LNA–LMCSs solutions with concentration of 100 mg/mL was added to each dish. After 2 h incubation, the medium was removed, and the cells were washed three times with cold PBS and fixed with freshly prepared 4% paraformaldehyde in PBS at room temperature for 10 min. Thereafter, cells were permeabilized in 0.1% Triton X-100/PBS, followed by twice wash with cold PBS. After three times wash with cold PBS, the cells were incubated with Hoechst 33342 for 20 min at room temperature to stain cell nuclei, followed by F-actin staining with Rhodamin-phalloidin for 40 min or by cell membrane staining with DiI for 10 min. The cells were washed three times with cold PBS and then preserved in blocking solution (glycerol:PBS, 1:1, v/v) for confocal laser scanning microscope (CLSM) observation.

2.13. Pharmacokinetics and statistical analysis

The pharmacokinetic parameters were calculated by the statistical moment method using the DAS 2.0 software. The data obtained from pharmacokinetic parameters were analyzed statistically by one-way analysis of variance and *t*-test using SPSS version 11.0 software. Results were reported as mean ± SD (SD: standard deviation). Values of $p < 0.05$, $p < 0.01$ and $p < 0.001$ were considered to be significant, highly significant and extremely significant, respectively.

3. Results and discussion

3.1. Synthesis and characterization of α-LNA–LMCS

α-LNA–LMCSs were successfully obtained by esterification and they were characterized by FTIR, ^{1}HNMR. LMCS has three free hydroxyl groups on each repeating disaccharide unit. Hydrophobic CS derivatives can be easily synthesized by replacing the hydroxyl groups with hydrophobic groups. In the presence of 4-dimethylamiopryidine, LMCS was modified by replacing the hydroxyl groups of the GlcA and GalNAc unit with α-linolenic acid groups to produce hydrophobically modified LMCSs. FTIR spectra of α-LNA–LMCSs proved that all samples had successfully undergone the esterification of the hydroxyl groups in the repeating disaccharide of glucuronic acid (GlcA) and *N*-acetylgalactosamine (GalNAc) (Fig. 3), as indicated by C=O stretching at 1738 cm^{-1}, —OH stretching at 3300 cm^{-1}, and C=C bonds at 2930 cm^{-1}. The absorption peak at 3300 cm^{-1} related to stretching vibration of hydroxyl group became weak owing to the modification with esterification, and the characteristic peak of ester group at 1752 cm^{-1} increased with increasing feed ratio of α-linoleoyl chloride. Therefore, it is demonstrated that LMCS was modified successfully by α-LNA.

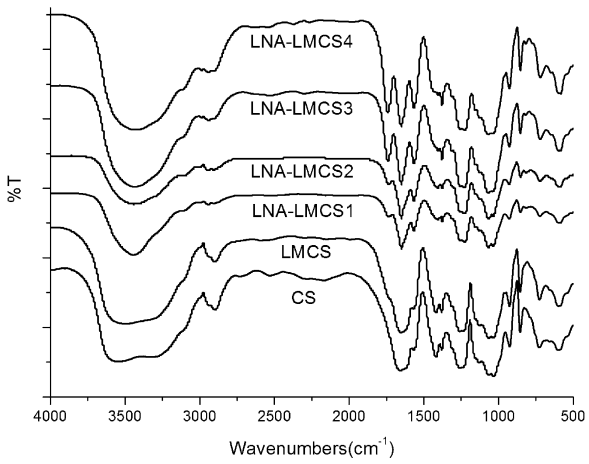

Fig. 3. FTIR spectra of CS and its derivatives.

The successful preparation of α-LNA–LMCSs was also confirmed by ^{1}HNMR (Fig. 4). Fig. 4A presented the typical ^{1}HNMR spectrum of α-linolenic acid in $CDCl_3$. The signals from the chemical shifts of δ 0.85–2.81 ppm were assigned to the methylene protons, and methine protons in α-LNA chain, and so did the peak at δ 5.34 ppm. The proton signals of chondroitin sulfate were observed in the range of δ 3.12–4.75 ppm belonging to the methine or methylene of disaccharide units, and the peak at δ 1.97 ppm belonging to the N-acetyl group of GalNAc, as shown in Fig. 4B. After partial esterification, the peak in the range of δ 3.12–4.75 ppm which is the characteristic signals for methine and methylene protons of LMCS was still remained,meanwhile, the new peak at δ 0.85–2.11 ppm was thought to be the methine and methylene protons of α-LNA chain (Fig. 4C–F). The sharp peak at δ 1.97 ppm was attributed to the acetamide groups of LMCS and the methyl group of α-LNA. The methylene and methine proton signals of the α-LNA at δ 5.34 ppm were extremely broad and weak in the α-LNA–LMCS polymers, it may be due to the content of α-LNA was low and the mobility of the α-LNA in water was poor. These results indicated that esterification was certainly preceded.

The degree of substitution (DS) was estimated by ^{1}HNMR and the values were listed in Table 1. The DS values of these polymers were calculated from the integration value of protons of LMCS moiety at δ 3.12–4.75 ppm and that of protons of α-LNA moiety observed at δ 0.85–2.11 nm. These values meant the average number of hydroxyl groups on the disaccharides of LMCS that had reacted with α-LNA. The DS of these copolymers ranged from 0.034 to 0.123. These results indicated that the α-LNA was introduced as the side chains of LMCS, and therefore, they could be regarded as branched LMCS.

To investigate the thermal decomposition of the α-LNA–LMCS in the solid state, TGA and DSC experiments were performed in the presence of a nitrogen gas flow and the results were shown in Fig. 5. The initial weight losses of CS and its derivatives were about 5–11% at the temperature from 30 to 150 °C. The degradation of CS and its derivatives started at 200 °C, and from then on, the heweight losses were about 50%. The DSC thermogram of LMCS exhibited one endothermic and one exothermic transition at 90.4 °Cand 221.7 °C in Fig. 5B, respectively. The DSC thermogram of α-LNA revealed one endotherm at 292.0 °C in Fig. 5C. However, cross linked α-LNA–LMCSs

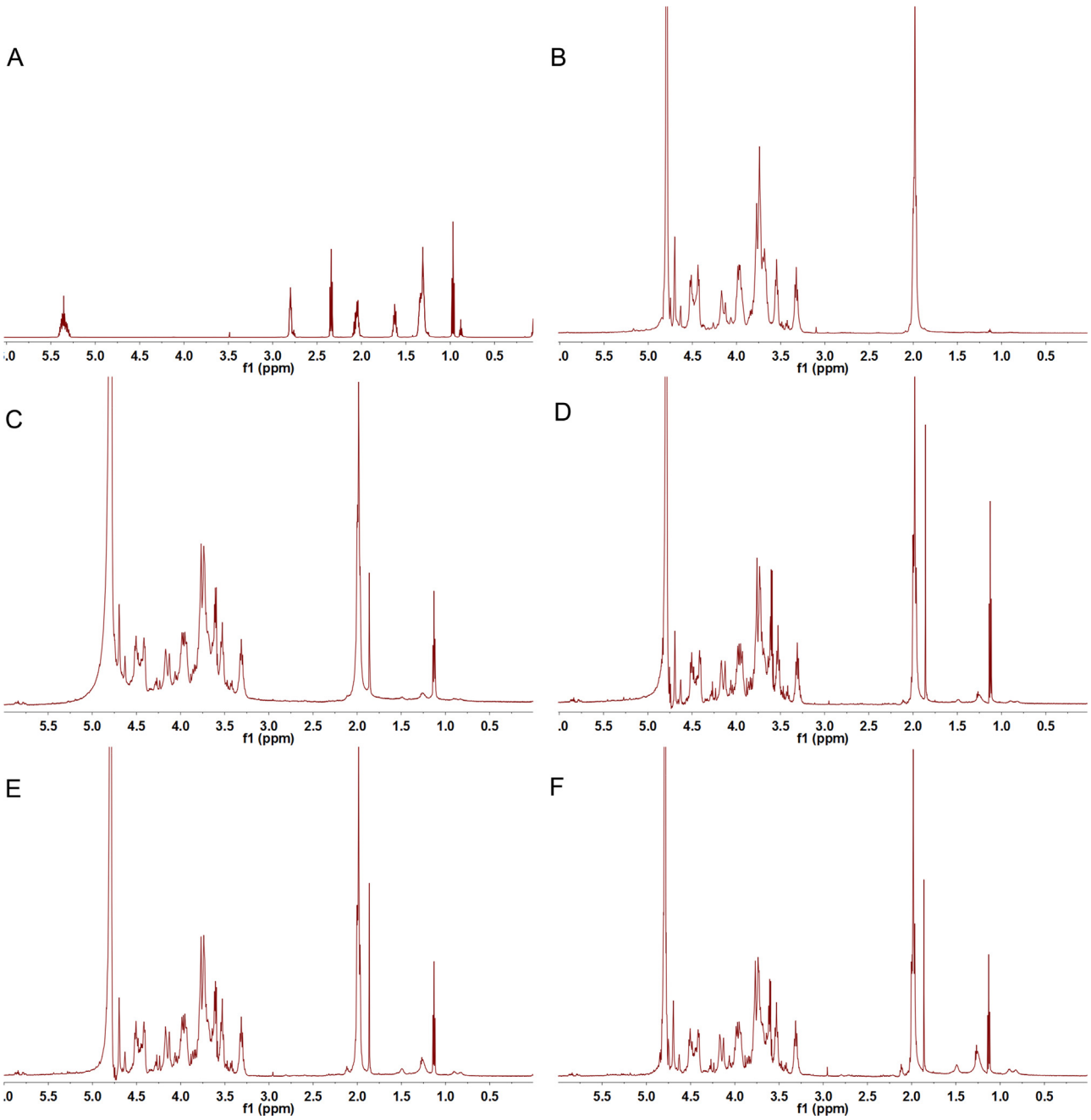

Fig. 4. The ^{1}H NMR spectra of α-LNA, CS and its derivatives. (A) α-LNA, (B) LMCS, (C) LNA–LMCS1, (D) LNA–LMCS2, (E) LNA–LMCS3 and (F) LNA–LMCS4.

Table 1
Properties of α-LNA–LMCS micelles ($n = 3$).

Formulation	d (nm)	ζ (mV)	DS (%)	CAC (mg/mL)
LNA–LMCS1	78.7 ± 4.8	−35.9 ± 0.3	0.034	0.0205
LNA–LMCS2	91.9 ± 4.7	−33.7 ± 1.8	0.057	0.0168
LNA–LMCS3	103.2 ± 7.1	−34.4 ± 0.5	0.085	0.0164
LNA–LMCS4	117.7 ± 5.1	−25.4 ± 1.0	0.123	0.0164

d: Mean particle diameter measured by the dynamic laser light scattering technique.
ζ: The Zeta potential of α-LNA–LMCS micelles in deionised water (1 mg/mL).
DS: Degree of substitutionexpressed as mole α-LNA and LMCS.
CAC: Critical aggregation concentration determined by fluorescence spectroscopy.

exhibited two endotherm transitions at about 70.0 °C and 265.0 °C and a large exothermic transition at about 205.0 °C (Fig. 5E–H). As no significant mass loss was found at the temperature from 30.0 to 150.0 °C by TGA (5–11%), the first broad endothermic transition changed at 70 °C may be associated with some adsorbed water (or ethanol) removal or some phase change in the polysaccharide (Piai et al., 2009). The second endothermic transition of α-LNA–LMCSs occurring in the range of 250.0 to 300.0 °C may be related to the removal of α-LNA from α-LNA–LMCS, and it was different in the ΔH value among α-LNA–LMCSs containing different ratios of α-LNA/LMCS. The

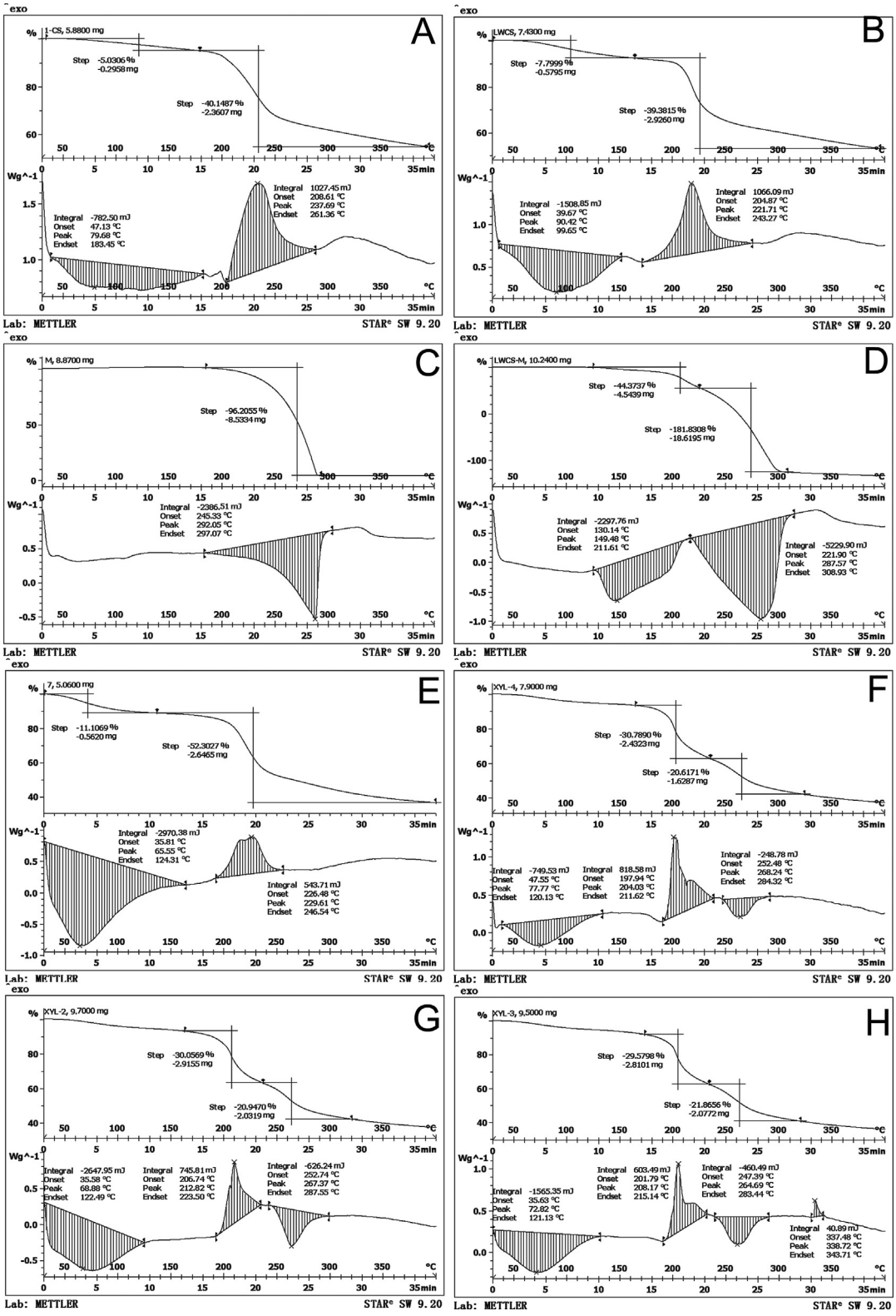

Fig. 5. TGA–DSC curves of CS and its derivatives. (A) CS, (B) LMCS, (C) α-LNA, (D) α-LNA and LMCS mixture, (E) LNA–LMCS1, (F) LNA–LMCS2, (G) LNA–LMCS3 and (H) LNA–LMCS4.

exothermic transition of CS and LNA–LMCSs occurring at 200.0 to 250.0 °C was accompanied with about 20% mass loss as shown in the respective TGA curves, which was due to the decomposition of glucuronic acid and *N*-acetylgalactosamine units (Guinesi and Cavalheiro, 2006). An endothermic transition at 200.0–250.0 °C was showen in the DSC curves of α-LNA–LMCSs, which was not present in that of LMCS. Comparison of endothermic and exothermic transition of LMCS and α-LNA–LMCS, it can be concluded that some polymorphic changes have occurred after modification of LMCS with α-LNA.

3.2. Characterization of α-LNA–LMCS micelles

The size and size distribution of α-LNA–LMCS micelles were characterized by laser light scattering and α-LNA–LMCS micelles exhibited a mean particle diameter of about 78–117 nm for the different conjugates (Table 1). As shown in Fig. 6, the size distributions of micelles were unimodal and the polydispersity indices were very low (<0.1), implying a narrow size distribution for all the conjugates. The laser light scattering results showed that three batches of micelles had no substantial difference, which demonstrated that the preparation process was reproducible and stable. TEM was used to visualize directly the size and morphology of α-LNA–LMCS micelles (Fig. 7). Smooth sphere morphology and a uniform size distribution of α-LNA–LMCS micelles were observed. The diameter of micelles observed by TEM appeared to be not consistent with the results determined by laser light scattering measurement, which was probably caused by the different mechanisms of the two methods. Since laser light scattering method involves the measurement of size in the aqueous state, micelles were highly hydrated and the size detected by laser light scattering was hydrated diameter, which was usually larger than their real dimensions. Whereas, the size observed by TEM was obtained at the dried state of the sample. This indicated that the diameter observed by TEM method was consistently smaller than the real dimensions.

Zeta potential is an important parameter to predict the physical storage stability of micellar systems. A higher absolute value of the zeta potential may provide a repelling force between the micelles, indicating the better stability of this colloidal system (Teeranachaideekul et al., 2007). In general, the absolute zeta potential values greater than 30 mV signify long-term stability of aqueous dispersion. As shown in Table 1, the LNA–LMCS1, LNA–LMCS2 and LNA–LMCS3 micelles had relatively high negative zeta potentials greater than −30 mV. The negative zeta potential indicated that the micelle surface was negatively charged. This high negative charge was attributed to the presence of ionized carboxyl groups and sulfonic acid groups of α-LNA–LMCS on the micelle surface, resulting in improved micelles stability as the result of internal charge-charge repulsion. In our study, the α-LNA–LMCS micelles were stable when sealed and stored at 4 °C for one month.

The CACs of α-LNA–LMCSs were determined by fluorescence technology in the presence of pyrene as a fluorescence probe (Mi et al., 2011). When micelles formed, pyrene molecules preferably located inside or close to the hydrophobic domains of micelles rather than the aqueous phase, resulting in different photophysical characteristics. The CACs of α-LNA–LMCSs can be obtained by plotting the I_{372}/I_{383} ratio of each curve in the excitation spectra versus log concentration of the polymer. The maximum change in the slope represents the formation of α-LNA–LMCS micelles (Fig. 8). Using this method, the CACs of α-LNA–LMCSs were determined (Table 1). The CAC values of α-LNA–LMCSs (about 0.016 mg/mL) were lower than those of low molecular weight surfactants and amphiphilic peptides, e.g., 1.0 mg/mL for deoxycholic acid (Kratohvil et al., 1986), 2.3 mg/mL for sodium dodecyl sulfate in water (Rahman and Brown, 1983) and 1.35 mg/mL for amphiphilic peptides with arginines and valines (Ryu et al., 2011), indicating that α-LNA–LMCSs were a novel kind of amphiphilic polymers and could form the stable self-assembling micelles in water at low concentration. The relatively low CAC may render the stability of the micelles upon dilution *in vivo* and *in vitro*, which is important for the oral bioavailability of α-LNA–LMCS.

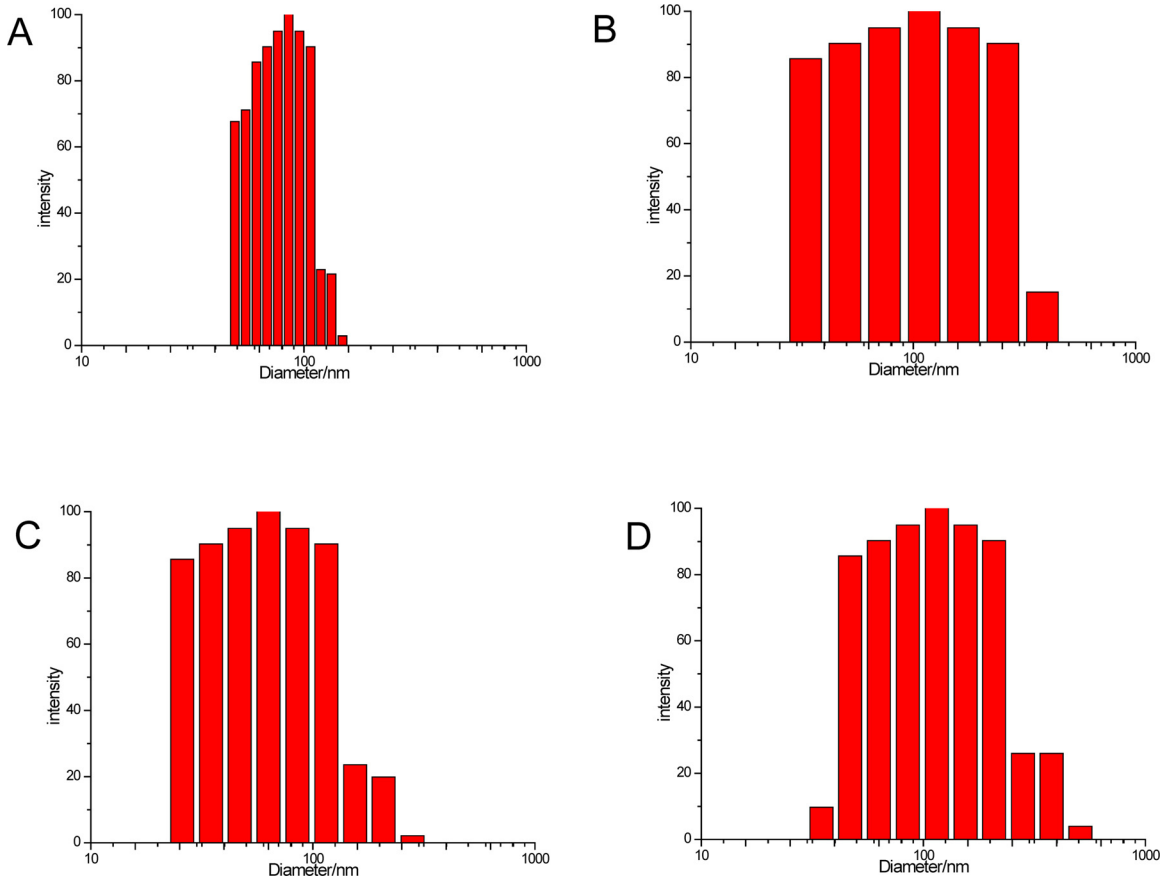

Fig. 6. Histograms of the size and size distribution of α-LNA–LMCS micelles (A) LNA–LMCS1; (B) LNA–LMCS2; (C) LNA–LMCS3 and (D) LNA–LMCS4.

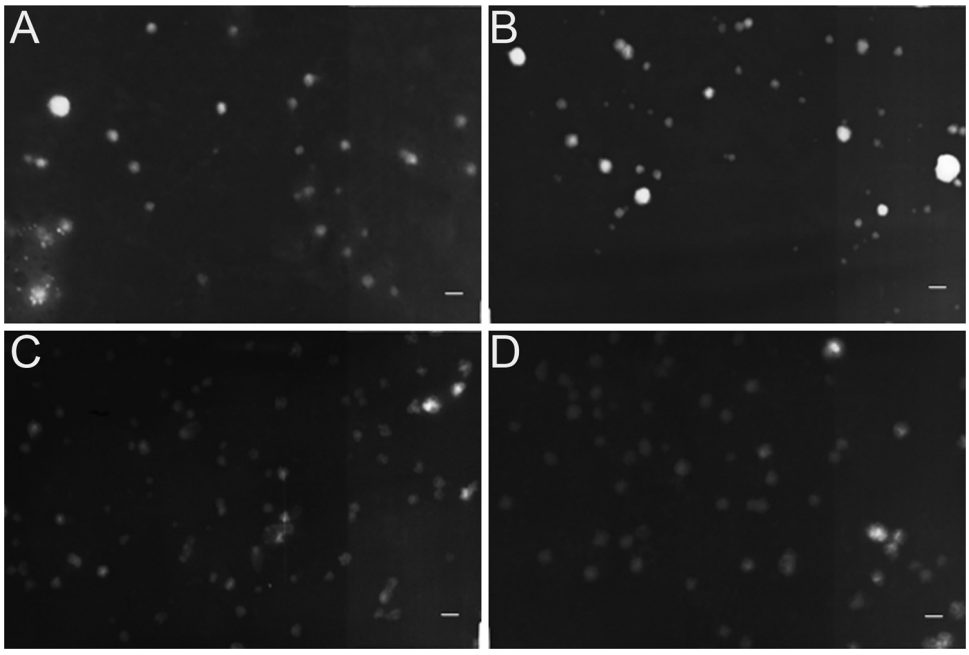

Fig. 7. TEM images of self-aggregates of α-LNA–LMCS micelles (A) LNA–LMCS1, (B) LNA–LMCS2, (C) LNA–LMCS3 and (D) LNA–LMCS4 (0.5 mg/mL). The bars indicate 100 nm.

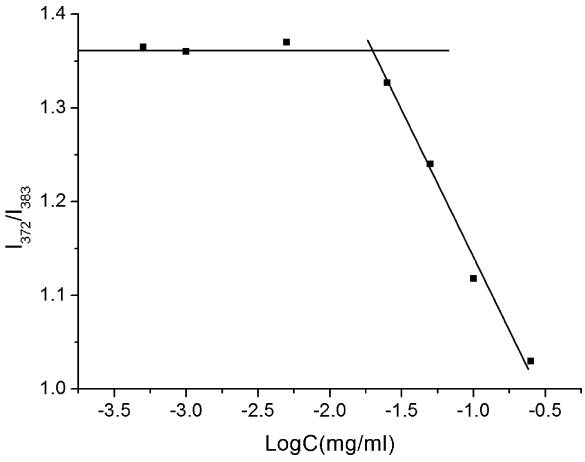

Fig. 8. Plot of the fluorescence intensity ratio of I_{372}/I_{383} from excitation spectra as a function of α-LNA–LMCS1 concentration.

3.3. In vivo *absorption efficacy assessment*

The absorptions of CS and its derivatives were evaluated *in vivo* and the oral bioavailability of CS has been significantly improved. The absorptions of CS and its derivatives were evaluated by intragastric administration to rats at a single dose of 200 mg/kg. Normal CS and LMCS were also intragastric administered as controls. The plasma CS concentration-time profiles after administration to rats were shown in Fig. 9 and the pharmacokinetics parameters were summarized in Table 2. The peak concentration of CS and LMCS in plasma were 3.8 ± 0.5 mg/L and 6.8 ± 0.8 mg/L, respectively. The maximum concentration (C_{max}) of LNA–LMCS2 at 8.8 ± 2.3 h was 10.8 ± 0.5 mg/L, which was obviously higher than that of CS and LMCS. In this study, the terminal elimination half-life ($t_{1/2}$) of CS and LMCS were about 11.0 ± 2.4 h and 5.9 ± 2.9 h, respectively. In contrast, LNA–LMCS2 showed a much longer circulation time and its elimination $t_{1/2}$ was 18.8 ± 3.1 h, 3.2 times longer than that of LMCS, which may be due to its low ζ potential and moderate size (Li and Huang, 2008). The total body clearance (CL) of LNA–LMCS2 was

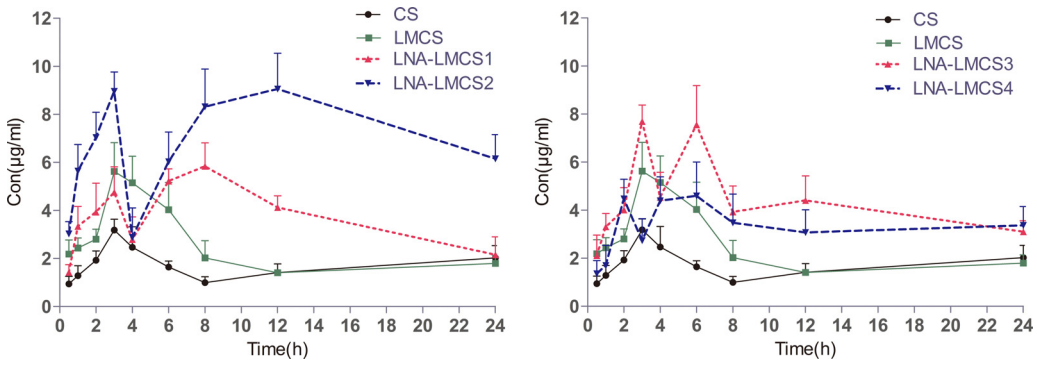

Fig. 9. The plasma CS concentration-time profile after administration in rats at a single equivalent dose of 200 mg/kg.

Table 2
Pharmacokinetic parameters of CS and its derivatives in rats at the equivalent 200 mg/kg dose ($n = 6$).

Parameters	CS	LMCS	LNA–LMCS1	LNA–LMCS2	LNA–LMCS3	LNA–LMCS4
AUC_{0-24} (mg/(L h))	40.0 ± 4.4	55.2 ± 4.4	89.9 ± 8.9$^{*\triangle}$	172.4 ± 20.9$^{**\triangle\triangle}$	102.7 ± 12.6$^{**\triangle}$	80.1 ± 16.9*
$AUC_{0-\infty}$ (mg/(L h))	63.4 ± 13.2	67.1 ± 12.3	126.8 ± 18.8$^{*\triangle}$	464.7 ± 54.8$^{**\triangle\triangle}$	158.6 ± 28.3$^{\triangle}$	163.0 ± 34.6$^{*\triangle}$
MRT_{0-24} (h)	12.4 ± 2.0	10.0 ± 1.7	10.5 ± 1.4	12.0 ± 0.6	11.0 ± 0.9	11.8 ± 1.3
$MRT_{0-\infty}$(h)	27.0 ± 8.2	15.7 ± 3.3	21.3 ± 5.9	21.0 ± 6.0	26.0 ± 7.2	22.6 ± 6.3
$t_{1/2}$ (h)	11.0 ± 2.4	5.9 ± 2.9*	11.2 ± 2.6$^{\triangle}$	18.8 ± 3.1$^{\triangle\triangle}$	15.3 ± 3.5$^{\triangle}$	11.5 ± 2.4$^{\triangle}$
T_{max} (h)	3.2 ± 0.5	4.0 ± 1.4	5.2 ± 3.2	8.8 ± 2.3$^{*\triangle}$	4.5 ± 1.7	4.5 ± 1.9
$CL_{z/F}$ (L/(h kg))	3.3 ± 0.7	3.1 ± 0.6	1.7 ± 0.5$^{**\triangle}$	0.6 ± 0.4$^{**\triangle\triangle}$	1.4 ± 0.7$^{*\triangle}$	1.5 ± 0.7$^{*\triangle}$
$V_{z/F}$ (L/kg)	53.0 ± 7.2	25.1 ± 3.9*	23.6 ± 3.1*	11.2 ± 2.4*	26.3 ± 4.2*	27.0 ± 5.8
C_{max} (mg/L)	3.8 ± 0.5	6.8 ± 0.8*	7.2 ± 1.5**	10.8 ± 0.5$^{**\triangle\triangle}$	9.4 ± 1.2$^{**\triangle}$	6.7 ± 0.7*

AUC_{0-24}: area-under-the-curve from time 0 to 24 h; $AUC_{0-\infty}$: area-under-the-curve from time 0 to infinity; MRT_{0-24}: mean residence time from time 0 to 24 h; $MRT_{0-\infty}$: mean residence time from time 0 to infinity; $t_{1/2}$: half-life time; T_{max}: the time at maximum plasma concentration; $V_{z/F}$: volume of distributionduring the terminal phase; $CL_{z/F}$: total body clearance; C_{max}: the maximum plasma concentration. $^{*}p < 0.05$ vs CS; $^{**}p < 0.001$ vs CS; $^{\triangle}p < 0.05$ vs LMCS $^{\triangle\triangle}p < 0.05$ vs LMCS.

0.6 ± 0.4 L/(h kg), which is 5.6 times and 5.3 times smaller than that of CS and LMCS, respectively. Moreover, the mean residence time (MRT) of LNA–LMCS2 in the plasma was 12.0 ± 0.6 h, 1.2 times longer than that of LMCS. Altogether, LNA–LMCS2 had longer $t_{1/2}$ and MRT, lower CL than LMCS in rats. At the same time, the AUC_{0-24} of LNA–LMCS2 after intragastric administration was 172.4 ± 20.9 mg/(L h), extremely higher than that of CS, 40.0 ± 4.4 mg/(L h) and LMCS, 55.2 ± 4.4 mg/(L h), respectively, ($p < 0.001$). The result indicating that the oral bioavailability of CS was significantly improved after esterification. According to the previous report (Lee et al., 2001), it is believed that the self-assembling micelles of amphiphilic polysaccharide can improve the oral bioavailability of polysaccharides.

The oral bioavailability of α-LNA–LMCSs was affected by two main factors: the molecular weight and the hydrophobicity. The hydrophobicity of α-LNA–LMCSs is determined by the coupling ratio of α-LNA to LMCS. Both the low molecular weight and the perfect coupling ratio are important to increase its permeability passing through the mucous cell layer in the intestinal tract. In the pharmacokinetic results of CS and its derivatives, the C_{max} of LMCS was obviously higher than that of CS, which means that the low molecular weight is beneficial to the oral bioavailability of CS. Among the α-LNA–LMCSs, LNA–LMCS2 showed the highest oral bioavailability. This result indicated that too high coupling ratio of α-LNA to LMCS may affect the solubility of α-LNA–LMCS and the formation of micelles, which then lead to the reduction of oral bioavailability.

3.4. Cytotoxicity studies in Caco-2 and HT29 cells

Before the transport studies, the cellular toxicities of the CS and its derivatives were evaluated for two objectives: (1) to obtain a preliminary estimation of the safety of CS and its derivatives, and (2) to determine the concentrations that could interfere with the cellular metabolism for further studies in Caco-2 and HT29 cells.

The effect of CS and its derivatives on the cellular viability of Caco-2 and HT29 cells were summarized in Fig. 10. The cytotoxicity of all the samples showed concentration-dependent manors. Cells treated by CS, LMCS, LNA–LMCS1 and LNA–LMCS2 showed high viabilities, even at the high concentration of 500 /mL. On the other hand, LNA–LMCS3 and LNA–LMCS4 exhibited a little toxicity to Caco-2 cells at high concentrations. At the concentration of 100 μg/mL, the cell viability of all the conjugates was up to 80%. Therefore, 100 μg/mL was selected as the threshold concentration for further Caco-2 experiments to ensure safety. These results suggested that the modified LMCS had no significant cytotoxicitic effect on Caco-2 and HT29 cells.

3.5. Effect of CS and its derivatives on TEER of Caco-2 cell monolayers

It was reported that measurements of TEER of Caco-2 cell monolyers could predict the paracellular permeability of drugs (Van der Merwe et al., 2004). As the tight junctions open, the TEER of Caco-2 cell monolayers would be significantly reduced, due to ion passages through the paracellular route. The effect of CS and its derivatives of various degrees of substitution and the polysaccharide concentrations on TEER of Caco-2 cell monolayers were summarized in Fig. 11. As shown in Fig. 11, the TEER values of Caco-2 cell monolayers incubated with LNA–LMCS2, LNA–LMCS3 and LNA–LMCS4 showed significant differences compared to that of the control groups incubated with CS and LMCS. This indicated that LNA–LMCS2, LNA–LMCS3 and LNA–LMCS4 have some effects on the opening of intercellular tight junctions(Lin et al., 2007). CS and its derivatives could decrease the TEER values in a concentration-dependent manner. The magnitude of increase in permeability (decrease in TEER) was consistent with the previous reports on the effect of drugs on TEER of Caco-2 cell layers(Yeh et al., 2011). After the CS and its derivatives were removed, the cells were repeatedly washed and subsequently supplied with fresh medium, and an increase in resistance towards the initial values was found in all the groups at 24 h (Fig. 12). The TEER recovery was obvious and nearly reversible within 24 h after the cells were treated with CS and its derivatives at low concentrations of 4–100 μg/mL for 2 h. However, the TEER recovery was partially reversible at concentration of 500 μg/mL. For the subsequent transport study, the concentration of 100 μg/mL was chosen because it was the most effective dose for TEER recovery. These observations indicated that the LNA–LMCS2, LNA–LMCS3 and LNA–LMCS4 could transiently open the tight junctions between Caco-2 cells, indicating that the mechanism of α-LNA–LMCSs transport was paracellular transport via tight junctions. Nevertheless, this result was inconsistent with the previous literature, in which Lin et al. had found that particles with negative charges could not disrupt tight junctions while particles with positive charges had the ability to open tight junctions (Lin et al., 2007).

3.6. Evaluation of CS and its derivatives transporting across Caco-2 cell monolayers

In recent years, the Caco-2 cell line has become a popular model of the intestinal mucosa because these cells have a colonic origin and express transporters that are normally found in the intestinal mucosa(Yee, 1997). To further evaluate the direct ability of esterification of LMCS in increasing the permeability of hydrophilic macromolecules, we studied the effect of DS of α-LNA on the transportation of hydrophilic macromolecules across Caco-2 cell

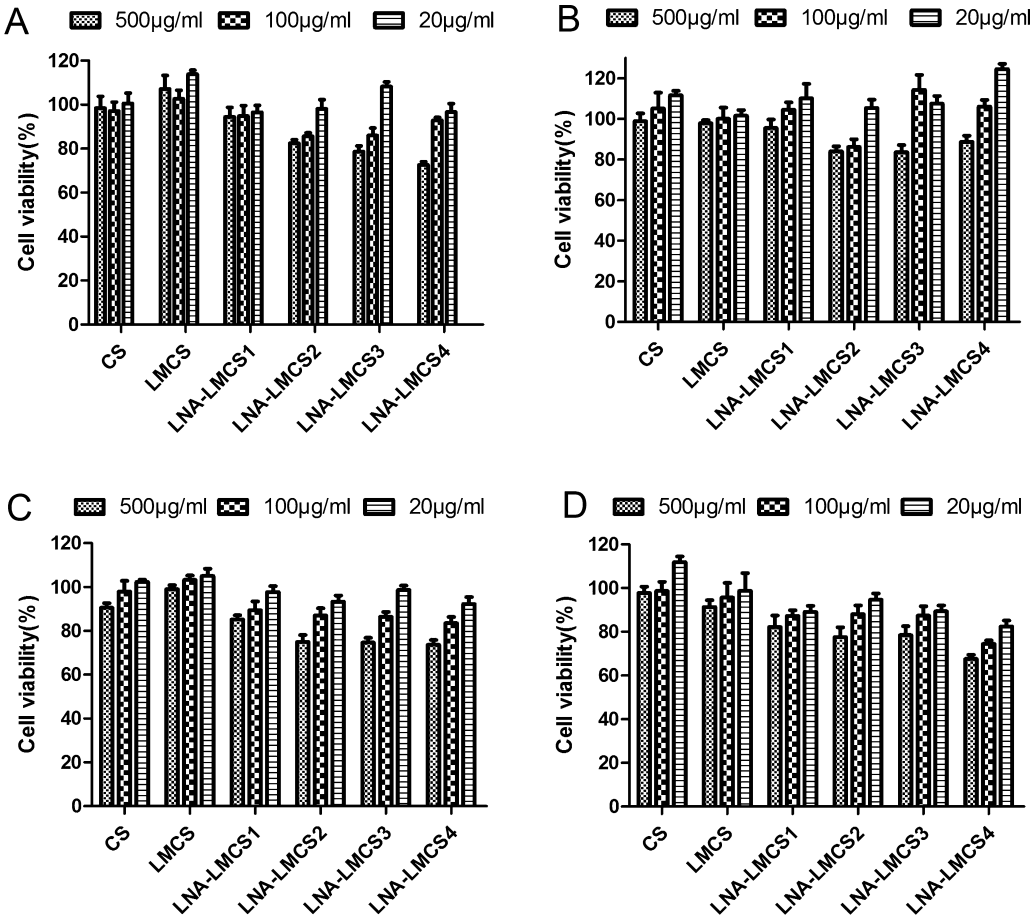

Fig. 10. Cytotoxicity of CS and its derivatives against caco-2 cells and HT29 cells after treatment for 48 h and 72 h: (A) HT29 cells, 48 h. (B) HT29 cells, 72 h. (C) caco-2 cells, 48 h. and (D) caco-2 cells, 72 h.

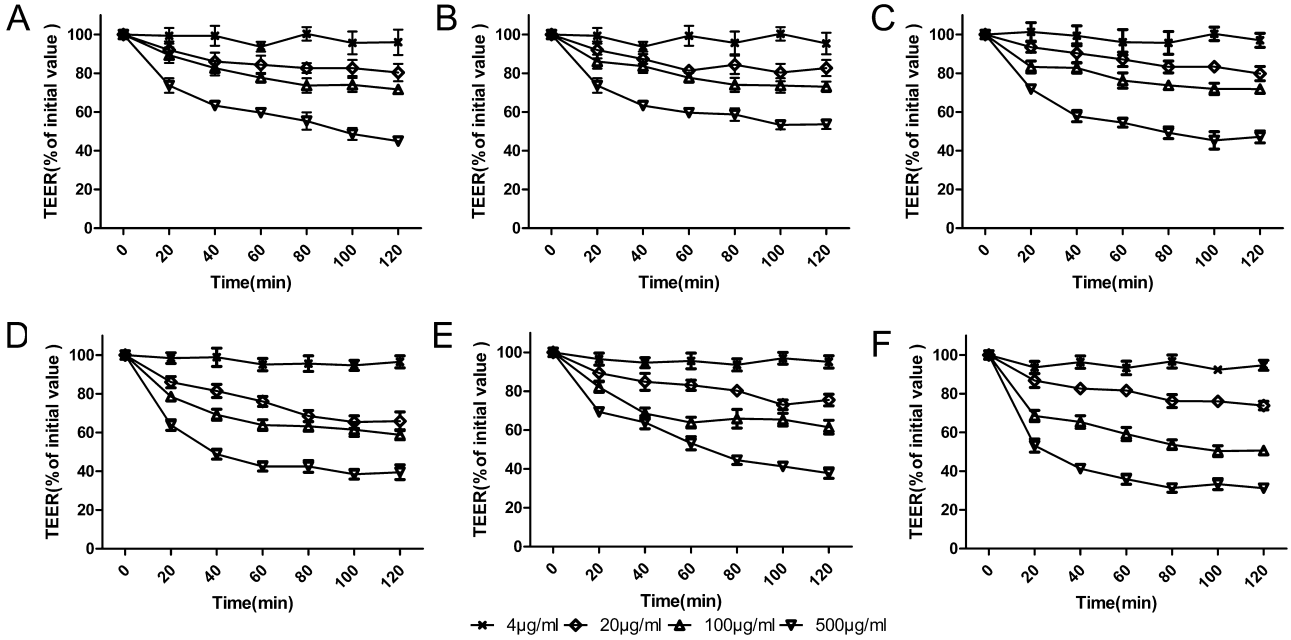

Fig. 11. The effect of CS and its derivatives on the TEER of Caco-2 cell monolayers: (A) LMCS, (B) α-LNA and LMCS mixture, (C) LNA–LMCS1, (D) LNA–LMCS2, (E) LNA–LMCS3 and (F) LNA–LMCS4 concentrations ranging from 4 to 500 μg/mL. ($n = 3$)

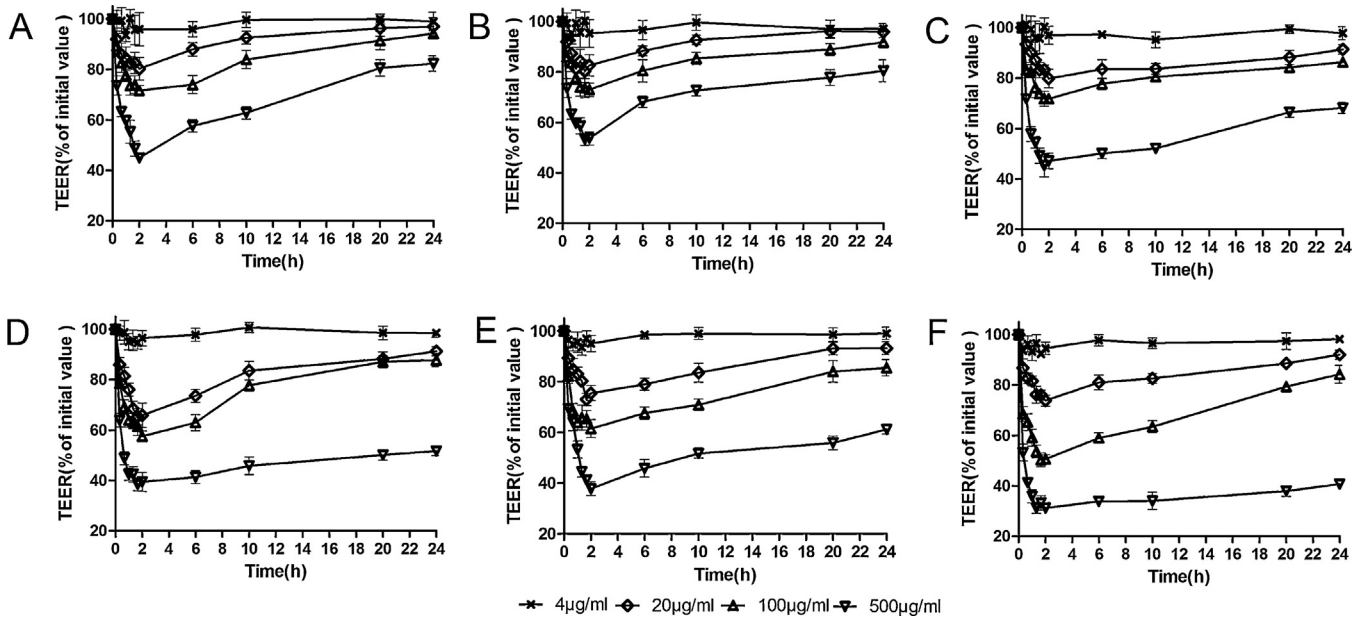

Fig. 12. The TEER recovery pattern of the Caco-2 cell monolayers: (A)LMCS, (B) α-LNA and LMCS mixture, (C) LNA–LMCS1, (D) LNA–LMCS2, (E) LNA–LMCS3 and (F) LNA–LMCS4 concentrations ranging from 4 to 500 μg/mL. ($n = 3$)

monolayers. The P_{app} were determined from apical to basolateral compartment through Caco-2 cell monolayers following the treatment with free CS and its derivatives, and the concentration for all test samples was 100 μg/mL. The results were depicted in Table 3. Excitingly, the efflux ratios of α-LNA–LMCSs were remarkably lower than that of CS or LMCS ($p < 0.05$), which indicated that α-LNA–LMCS micelles had inhibitory effect on P-glycoprotein (P-gp). The enhancing transport of α-LNA–LMCS micelles might be attributed to the transcytosis mechanism, entering the Caco-2 cells at the apical surface of the monolayer via endocytosis and afterward leaving the cells by exocytosis at the basolateral surface(Sang Yoo and Gwan Park, 2004), which was in agreement with earlier reports of mPEG–PLA micelles encapsulating lower bioavailability drug, Salmon calcitonin(Li et al., 2012). In addition, it was observed that the $P_{app(BL-AP)}$ of LNA–LMCSs had no significant difference compared with that of free CS or LMCS. The $P_{app(AP-BL)}$ of LNA–LMCS2 was 2.2 times of that of free CS, indicating that the improvement of permeability of CS may be not only dependent on the transcellular transport through the cell membrane, but also paracellular transport from the tight junction to the lateral space. Based on these results and the *in vivo* efficacy study, it was deduced that the modification of LMCS with α-LNA improved its intestinal absorption through the enhancement of the transcellular and paracellular transport across intestinal cells.

Table 3
The transport of CS and its derivative across Caco-2 cell monolayers ($n = 3$).

Samples	P_{app} (10^{-6} cm/s)		Efflux ratio	R
	AP–BL	BL–AP		
CS (control)	3.7 ± 0.4	8.4 ± 1.0	2.3 ± 0.5	–
LMCS	4.8 ± 0.8	10.8 ± 1.7	2.3 ± 0.0	1.3
LNA–LMCS1	$5.4 \pm 0.8^{*}$	8.2 ± 1.0	$1.6 \pm 0.1^{*\triangle}$	1.5
LNA–LMCS2	$8.0 \pm 0.8^{**\triangle}$	10.6 ± 0.8	$1.3 \pm 0.1^{**\triangle\triangle}$	2.2
LNA–LMCS3	5.0 ± 0.4	7.9 ± 0.6	$1.6 \pm 0.1^{*\triangle}$	1.4
LNA–LMCS4	4.9 ± 0.2	7.1 ± 0.2	$1.4 \pm 0.1^{**\triangle\triangle}$	1.3

P_{app} is the apparent permeability coefficient of CS and its derivative across Caco-2 cell monolayers from AP to BL; R is the absorption enhancement ratio. $^{*}p < 0.05$ vs CS; $^{**}p < 0.001$ vs CS; $^{\triangle}p < 0.05$ vs LMCS; $^{\triangle\triangle}p < 0.001$ vs LMCS.

3.7. Paracellular transport of 5-AMF labeled CS and its derivatives

The solvent used for the labeling of the carbohydrates in the current study was an important parameter because of the solubility of 5-AMF. The 5-AMF was soluble at alkaline pH, while had a poor solubility in acidic LNA–LMCS micellar solutions. The labeling reaction could be conducted to promote formation of ammine in acidic media, whereas not carried out in alkaline solutions. Finally, we chose 50% ethanol, 50% water solution and low concentrations of 5-AMF as the reaction system and overcame this solubility problem.

As shown in Fig. 13, thin-layer chromatography of the filtrate revealed two bands and one spot after amidization: the top bands, middle broad bands and origin spots were recognized as 5-AMF, 5-AMF copolymer and labeled CS and its derivatives, respectively. 5-AMF labeled CS and its derivatives exhibited different R_f values from that of the free 5-AMF molecules or the 5-AMF copolymer. Therefore, CS and its derivatives were successfully labeled with 5-AMF. After dialysis and filtration, thin-layer chromatography of the filtrate revealed only one spot, neither free 5-AMF norits copolymers was detected. Furthermore, it is demonstrated that the purified samples do not contain free 5-AMF molecules.

The intracellular uptakes of CS and its derivatives were studied with Caco-2 cells using confocal laser microscopy. Fluorescent images were taken by staining cell nuclei using Hoechst 33342 (blue part) and cell membranes using DiI (red part). Confocal micrographs (Fig. 14) revealed the colocalization of the 5-AMF labeled CS and its derivatives (green part) with intrinsic fluorescence after incubating with Caco-2 cells for 2 h. As shown in Fig. 14, the control cells were flat and well spread, with small lamellipodia, and maintained their typical shape and surface morphology, suggesting the cell motility. The confocal laser microscopy images indicated that Caco-2 control cells retained their viability, shape, and structure over the observation period. The 5-AMF labeled CS and its derivatives (green part) mainly accumulated around the cell membrane and intercellular space after incubation.

In addition, the stereoscopic technique utilizing the confocal laser microscopy images were introduced to determine the

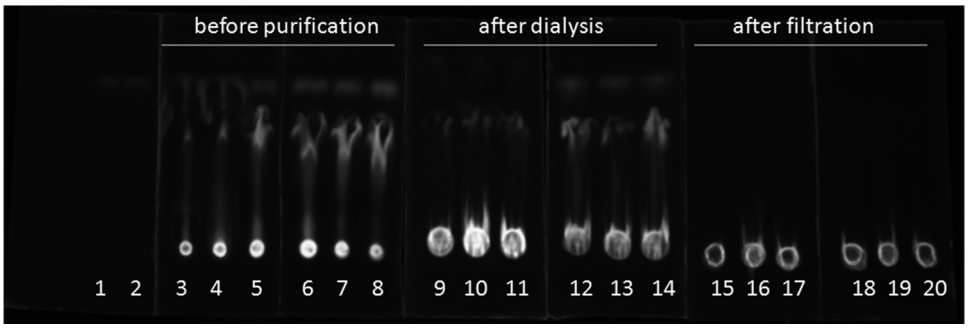

Fig. 13. Thin layer chromatogram of 5-AMF labeled CS and its derivatives. (1) 5-AMF; (2) 5-AMF and CS mixture; (3), (9), (15) 5-AMF labeled CS; (4), (10), (16) 5-AMF labeled LMCS; (5), (11), (17) 5-AMF labeled LNA–LMCS1; (6), (12), (18) 5-AMF labeled LNA–LMCS2; (7), (13), (19) 5-AMF labeled LNA–LMCS3; and (8), (4), (20) 5-AMF labeled LNA–LMCS4.

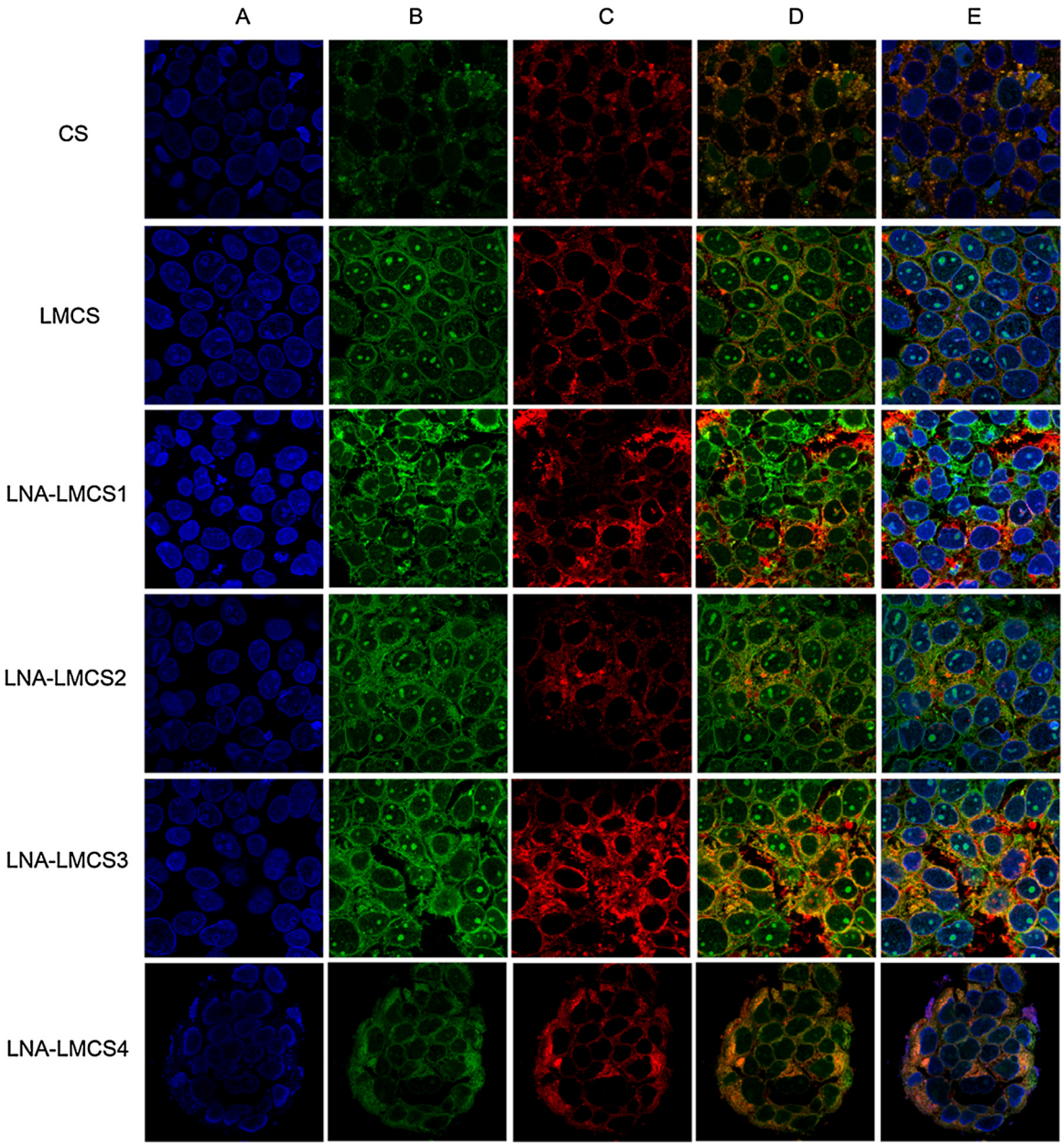

Fig. 14. Confocal laser scanning imaging of Caco-2 incubated with 5-AMF labeled CS and its derivatives. (A) cell nucleus stained with Hoechst 33342 (blue part), (B) 5-AMF labeled CS and its derivatives (green part), (C) cell membranes stained with DiI (red part), (D) merged B and C pictures and (E) merged A, B and C pictures. All images were taken at 126×magnification in oil (For interpretation of the references to color in this figure legend, the reader is referred to the web version of the article).

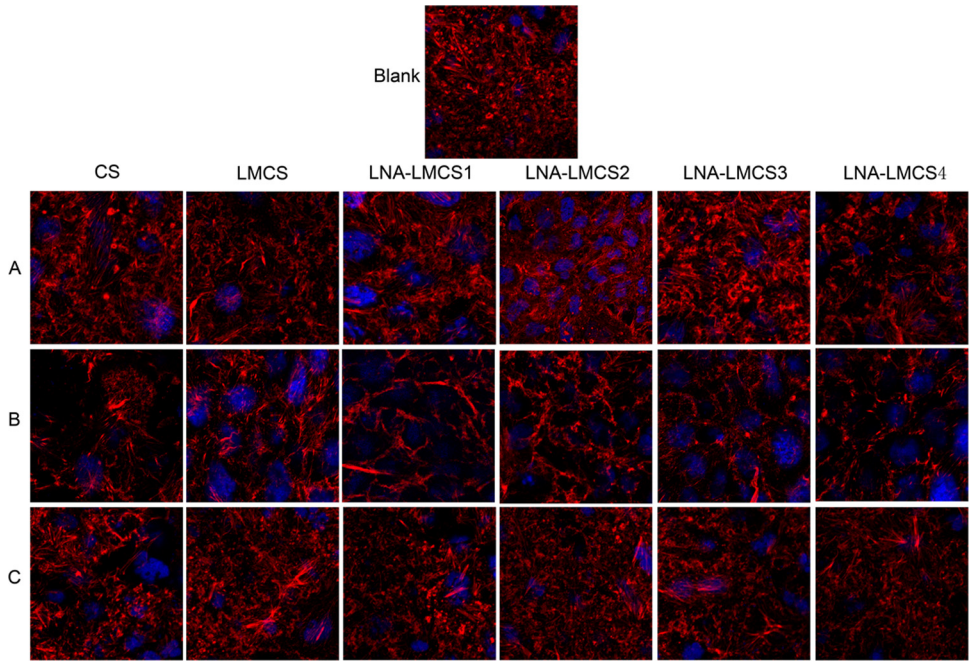

Fig. 15. F-actin staining of Caco-2 cell monolayers incubated with CS and its derivatives. (A) Caco-2 cell monolayers incubated with 100 μg/mL CS and its derivatives for 2 h; (B) Caco-2 cell monolayers incubated with 500 μg/mL CS and its derivatives for 2 h and (C) after incubated with 500 μg/mL CS and its derivatives for 2 h, cells were carefully washed twice with PBS and incubated 24 h with fresh culture medium. All images were taken at 126× magnification in oil.

subcellular distribution of CS and its derivatives at an organelle level. As shown in Fig. 14, a small amount of CS and LMCS aggregated in the intercellular space of Caco-2 monolayer after incubating, whereas all the 5-AMF labeled α-LNA–LMCSs were detected clearly on intercellular space of Caco-2 monolayers. Fig. 14 also showed that the cellular uptake of LNA–LMCS2 through the monolayer membrane was more rapid than that of other LNA–LMCS micelles. Therefore, it is indicated that modification of LMCS with α-LNA improved its intestinal absorption through the enhancement of the permeability across intestinal cells.

To visually investigate the possible transepithelial transport route of CS and its derivatives, the effects of various CS conjugates on the distribution of F-actin by specific staining with fluorescent phalloidin were also observed by CLSM. As shown in Fig. 15, control cells exhibited a regular distribution of actin filaments over the cell monolayer. Treatment with CS and its derivatives of 100 μg/mL for 2 h did not reduce the staining and alter the distribution of F-actin, but the monolayer treated with CS and its derivatives of 500 μg/mL appeared to have lost staining slightly. In the monolayer treated with a high concentration of CS and its derivatives (500 μg/mL), F-actin relocalized to a certain extent to the vicinity of the cell membrane. The transformation of its striated pattern is the possible consequence of the mechanochemical stress imposed by the particles onto the epithelial membrane (Fu et al., 2008). Similar structural alterations of F-actin cytoskeleton can lead to condensation in pericellular bands, as previously observed under the effect of substances that disrupt the intestinal epithelial barrier (Xu et al., 2011). In general, the cytoskeletal pattern of F-actin molecules in the perijunctional region of intestinal epithelial cells tends to be either thickened and tightened (Tahara et al., 2011), or disrupted and modulated (Finamore et al., 2008) following incubation with enteric biomolecules or nanoparticles. As seen in Fig. 15B, no disruption in its cytoskeletal pattern was detected, although F-actin filament was partially withdrawn to the cell periphery. Each cell was still surrounded by other cells on average, as in agreement with the previous observations on the packing of confluent layers of Caco-2 cells (Moyes et al., 2010). After the CS and its derivatives were removed, F-actin filament was almost full recovery observed after 24 h. These results indicated that the introduction of α-LNA into the LMCS polymer backbone enhanced the hydrophobicity, which improved the hydrophobic interaction between the polymer and the cell membrane. These improvements helped LNA–LMCS2 to be an oral polysaccharide with excellent absorption.

Based on these results, it was concluded that: (1) the paracellular pathway was involved in the transepithelial transport of α-LNA–LMCS micelles and the modification of LMCS with α-LNA improved its intestinal absorption; (2) α-LNA–LMCS micelles prepared in the present study could alter the F-actin cytoskeleton and the tight junctions permeability of the Caco-2 cell monolayer, but they did not disrupt the overall integrity of the monolayer.

4. Conclusions

In this work, a new kind of amphiphilic polysaccharides, α-LNA–LMCSs, was prepared and the physicochemical properties of α-LNA–LMCSs in aqueous phases were investigated. The mean diameters of self-aggregates of α-LNA–LMCSs were in the range of 78–117 nm. The CACs of α-LNA–LMCSs were in the range of 0.027–0.065 mg/mL. The characteristics of narrow size distribution and relatively low CACs may contribute to the stability of the micelles upon dilution *in vivo* and *in vitro* and the improved oral bioavailability of CS. It was demonstrated that LNA–LMCS2 has better absorption via oral administration than normal CS and LMCS. The good oral absorption of CS derivatives were contributed to the conjugated α-LNA molecule constituent that could promote intestinal absorption by enhancing the hydrophobic properties of LMCS and increasing the interaction between LMCS and the intestinal membrane. Moreover, the transport of LNA–LMCS2 micelles across intestinal epithelial barrier was proved via paracellular pathway and endocytosis for the first time. In summary, this study suggested that LNA–LMCS2 with low cytotoxicity and high oral bioavailability would be a promising substitute for CS. Furthermore, this study provided a simple set of

strategies suitable for the oral delivery of macromolecules and polysaccharide drugs.

Acknowledgments

This work was supported by the "973" grant from the Ministry of Science and Technology of China (2012CB822102), Taishan scholar Scheme (Special Term Expert for Pharmacy) and the Natural Science Foundation of Shandong Province of China (No. ZR2011HL052).

References

Albert, C.M., Oh, K., Whang, W., Manson, J.E., Chae, C.U., Stampfer, M.J., Willett, W.C., Hu, F.B., 2005. Dietary alpha-linolenic acid intake and risk of sudden cardiac death and coronary heart disease. Circulation 112, 3232–3238.

Baici, A., Horler, D., Moser, B., Hofer, H.O., Fehr, K., Wagenhauser, F.J., 1992. Analysis of glycosaminoglycans in human serum after oral administration of chondroitin sulfate. Rheumatology International 12, 81–88.

Brenna, J.T., Salem Jr., N., Sinclair, A.J., Cunnane, S.C., 2009. alpha-Linolenic acid supplementation and conversion to n-3 long-chain polyunsaturated fatty acids in humans. Prostaglandins Leukotrienes and Essential Fatty Acids 80, 85–91.

Burdge, G.C., Calder, P.C., 2006. Dietary alpha-linolenic acid and health-related outcomes: a metabolic perspective. Nutrition Research Reviews 19, 26–52.

Campos, H., Baylin, A., Willett, W.C., 2008. Alpha-linolenic acid and risk of nonfatal acute myocardial infarction. Circulation 118, 339–345.

Cervigni, M., Natale, F., Nasta, L., Mako, A., 2012. Intravesical hyaluronic acid and chondroitin sulphate for bladder pain syndrome/interstitial cystitis: long-term treatment results. International Urogynecology Journal 23, 1187–1192.

Deepa, S.S., Kalayanamitra, K., Ito, Y., Kongtawelert, P., Fukui, S., Yamada, S., Mikami, T., Sugahara, K., 2007. Novel sulfated octa- and decasaccharides from squid cartilage chondroitin sulfate E: sequencing and application for determination of the epitope structure of the monoclonal antibody MO-225. Biochemistry 46, 2453–2465.

Delgado-Roche, L., Acosta, E., Soto, Y., Hernandez-Matos, Y., Olivera, A., Fernandez-Sanchez, E., Vazquez, A.M., 2013. The treatment with an anti-glycosaminoglycan antibody reduces aortic oxidative stress in a rabbit model of atherosclerosis. Free Radical Research 47, 309–315.

Duhem, N., Rolland, J., Riva, R., Guillet, P., Schumers, J.M., Jerome, C., Gohy, J.F., Preat, V., 2012. Tocol modified glycol chitosan for the oral delivery of poorly soluble drugs. International Journal of Pharmaceutics 423, 452–460.

Finamore, A., Massimi, M., Conti Devirgiliis, L., Mengheri, E., 2008. Zinc deficiency induces membrane barrier damage and increases neutrophil transmigration in Caco-2 cells. Journal of Nutrition 138, 1664–1670.

Fu, Y.Y., Sibley, E., Tang, S.C., 2008. Transient cytochalasin-D treatment induces apically administered rAAV2 across tight junctions for transduction of enterocytes. Journal of General Virology 89, 3004–3008.

Gabay, C., Medinger-Sadowski, C., Gascon, D., Kolo, F., Finckh, A., 2011. Symptomatic effects of chondroitin 4 and chondroitin 6 sulfate on hand osteoarthritis: a randomized, double-blind, placebo-controlled clinical trial at a single center. Arthritis & Rheumatology 63, 3383–3391.

Guinesi, L.S., Cavalheiro, É.T.G., 2006. The use of DSC curves to determine the acetylation degree of chitin/chitosan samples. Thermochimica Acta 444, 128–133.

Kim, S.K., Vaishali, B., Lee, E., Lee, S., Lee, Y.K., Kumar, T.S., Moon, H.T., Byun, Y., 2006. Oral delivery of chemical conjugates of heparin and deoxycholic acid in aqueous formulation. Thrombosis Research 117, 419–427.

Kotze, A.F., Luessen, H.L., de Leeuw, B.J., de Boer, A.G., Verhoef, J.C., Junginger, H.E., 1998. Comparison of the effect of different chitosan salts and *N*-trimethyl chitosan chloride on the permeability of intestinal epithelial cells (Caco-2). Journal of Controlled Release 51, 35–46.

Kratohvil, J.P., Hsu, W.P., Kwok, D.I., 1986. How large are the micelles of di-α-hydroxy bile salts at the critical micellization concentrations in aqueous electrolyte solutions? Results for sodium taurodeoxycholate and sodium deoxycholate Langmuir 2, 256–258.

Lee, Y., Nam, J.H., Shin, H.C., Byun, Y., 2001. Conjugation of low-molecular-weight heparin and deoxycholic acid for the development of a new oral anticoagulant agent. Circulation 104, 3116–3120.

Li, N., Li, X.R., Zhou, Y.X., Li, W.J., Zhao, Y., Ma, S.J., Li, J.W., Gao, Y.J., Liu, Y., Wang, X.L., 2012. The use of polyion complex micelles to enhance the oral delivery of salmon calcitonin and transport mechanism across the intestinal epithelial barrier. Biomaterials 33, 8881–8892.

Li, S.D., Huang, L., 2008. Pharmacokinetics and biodistribution of nanoparticles. Molecular Pharmacology 5, 496–504.

Lin, Y.H., Mi, F.L., Chen, C.T., Chang, W.C., Peng, S.F., Liang, H.F., Sung, H.W., 2007. Preparation and characterization of nanoparticles shelled with chitosan for oral insulin delivery. Biomacromolecules 8, 146–152.

Mi, Y., Liu, Y., Feng, S.S., 2011. Formulation of docetaxel by folic acid-conjugated D-alpha-tocopheryl polyethylene glycol succinate (Vitamin E TPGS(2k)) micelles for targeted and synergistic chemotherapy. Biomaterials 32, 4058–4066.

Mizuguchi, S., Uyama, T., Kitagawa, H., Nomura, K.H., Dejima, K., Gengyo-Ando, K., Mitani, S., Sugahara, K., Nomura, K., 2003. Chondroitin proteoglycans are involved in cell division of Caenorhabditis elegans. Nature 423, 443–448.

Mo, R., Xiao, Y., Sun, M., Zhang, C., Ping, Q., 2011. Enhancing effect of *N*-octyl-*O*-sulfate chitosan on etoposide absorption. International Journal of Pharmaceutics 409, 38–45.

Mohan, T., Kargl, R., Kostler, S., Doliska, A., Findenig, G., Ribitsch, V., Stana-Kleinschek, K., 2012. Functional polysaccharide conjugates for the preparation of microarrays. ACS Applied Materials & Interfaces 4, 2743–2751.

Moller, I., Perez, M., Monfort, J., Benito, P., Cuevas, J., Perna, C., Domenech, G., Herrero, M., Montell, E., Verges, J., 2010. Effectiveness of chondroitin sulphate in patients with concomitant knee osteoarthritis and psoriasis: a randomized, double-blind, placebo-controlled study. Osteoarthritis and Cartilage 18, S32–S40.

Mosmann, T., 1983. Rapid colorimetric assay for cellular growth and survival: application to proliferation and cytotoxicity assays. Journal of Immunological Methods 65, 55–63.

Moyes, S.M., Morris, J.F., Carr, K.E., 2010. Macrophages increase microparticle uptake by enterocyte-like Caco-2 cell monolayers. Journal of Anatomy 217, 740–754.

Muller, A.J., Letelier, M.E., Galleguillos, M.A., Molina-Berrios, A.E., Adarmes, H.H., 2010. Comparison of the antioxidant effects of synovial fluid from equine metacarpophalangeal joints with those of hyaluronic acid and chondroitin sulfate. American Journal of Veterinary Research 71, 399–404.

Nandini, C.D., Sugahara, K., 2006. Role of the sulfation pattern of chondroitin sulfate in its biological activities and in the binding of growth factors. Advances in Pharmacology 53, 253–279.

Nguemeni, C., Delplanque, B., Rovere, C., Simon-Rousseau, N., Gandin, C., Agnani, G., Nahon, J.L., Heurteaux, C., Blondeau, N., 2010. Dietary supplementation of alpha-linolenic acid in an enriched rapeseed oil diet protects from stroke. Pharmacological Research 61, 226–233.

Piai, J.F., Rubira, A.F., Muniz, E.C., 2009. Self-assembly of a swollen chitosan/chondroitin sulfate hydrogel by outward diffusion of the chondroitin sulfate chains. Acta Biomaterialia 5, 2601–2609.

Qian, S., Zhang, Q., Wang, Y., Lee, B., Betageri, G.V., Chow, M.S., Huang, M., Zuo, Z., 2013. Bioavailability enhancement of glucosamine hydrochloride by chitosan. International Journal of Pharmaceutics 455, 365–373.

Rahman, A., Brown, C., 1983. Effect of pH on the critical micelle concentration of sodium dodecyl sulphate. Journal of Applied Polymer Science 28, 1331–1334.

Reginster, J.Y., 2012. In people with hand osteoarthritis, chondroitin sulphate therapy for 6 months improves pain and function compared with placebo. Evidence-Based Medicine 17, 152–153.

Ryu, D.W., Kim, H.A., Song, H., Kim, S., Lee, M., 2011. Amphiphilic peptides with arginines and valines for the delivery of plasmid DNA. Journal of Cellular Biochemistry 112, 1458–1466.

Sakai, S., Akiyama, H., Sato, Y., Yoshioka, Y., Linhardt, R.J., Goda, Y., Maitani, T., Toida, T., 2006. Chondroitin sulfate intake inhibits the IgE-mediated allergic response by down-regulating Th2 responses in mice. Journal of Biological Chemistry 281, 19872–19880.

Salartash, K., Lepore, M., Gonze, M.D., Leone-Bay, A., Baughman, R., Sternbergh 3rd, W.C., Bowen, J.C., Money, S.R., 2000. Treatment of experimentally induced caval thrombosis with oral low molecular weight heparin and delivery agent in a porcine model of deep venous thrombosis. Annals of Surgery 231, 789–794.

Sang Yoo, H., Gwan Park, T., 2004. Biodegradable nanoparticles containing protein–fatty acid complexes for oral delivery of salmon calcitonin. Journal of Pharmaceutical Sciences 93, 488–495.

Sato, Y., Nakanishi, K., Tokita, Y., Kakizawa, H., Ida, M., Maeda, H., Matsui, F., Aono, S., Saito, A., Kuroda, Y., Hayakawa, M., Kojima, S., Oohira, A., 2008. A highly sulfated chondroitin sulfate preparation, CS-E, prevents excitatory amino acid-induced neuronal cell death. Journal of Neurochemistry 104, 1565–1576.

Sim, J.S., Zhao, H.L., Li, D.W., Cho, S.Y., Jeong, C.S., Lee, E.B., Kim, Y.S., 2005. Effects of saponins from the root bark of Aralia elata on the transport of chondroitin sulfate in Caco-2 cell monolayers and rats. Biological and Pharmaceutical Bulletin 28, 1043–1048.

Stark, A.H., Crawford, M.A., Reifen, R., 2008. Update on alpha-linolenic acid. Nutrition Reviews 66, 326–332.

Sugahara, K., Mikami, T., 2007. Chondroitin/dermatan sulfate in the central nervous system. Current Opinion in Structural Biology 17, 536–545.

Sugahara, K., Mikami, T., Uyama, T., Mizuguchi, S., Nomura, K., Kitagawa, H., 2003. Recent advances in the structural biology of chondroitin sulfate and dermatan sulfate. Current Opinion in Structural Biology 13, 612–620.

Tahara, K., Samura, S., Tsuji, K., Yamamoto, H., Tsukada, Y., Bando, Y., Tsujimoto, H., Morishita, R., Kawashima, Y., 2011. Oral nuclear factor-kappaB decoy oligonucleotides delivery system with chitosan modified poly(D, L-lactide-co-glycolide) nanospheres for inflammatory bowel disease. Biomaterials 32, 870–878.

Teeranachaideekul, V., Souto, E.B., Junyaprasert, V.B., Muller, R.H., 2007. Cetyl palmitate-based NLC for topical delivery of Coenzyme Q(10) – development, physicochemical characterization and in vitro release studies. European Journal of Pharmaceutics and Biopharmaceutics 67, 141–148.

Van der Merwe, S., Verhoef, J., Verheijden, J., Kotze, A., Junginger, H., 2004. Trimethylated chitosan as polymeric absorption enhancer for improved peroral delivery of peptide drugs. European Journal of Pharmaceutics and Biopharmaceutics 58, 225–236.

Xu, L.F., Xu, C., Mao, Z.Q., Teng, X., Ma, L., Sun, M., 2011. Disruption of the F-actin cytoskeleton and monolayer barrier integrity induced by PAF and the protective effect of ITF on intestinal epithelium. Archives of Pharmacal Research 34, 245–251.

Yang, K.W., Li, X.R., Yang, Z.L., Li, P.Z., Wang, F., Liu, Y., 2009. Novel polyion complex micelles for liver-targeted delivery of diammonium glycyrrhizinate: in vitro and in vivo characterization. Journal of Biomedical Materials Research Part A 88, 140–148.

Yao, H.J., Ju, R.J., Wang, X.X., Zhang, Y., Li, R.J., Yu, Y., Zhang, L., Lu, W.L., 2011. The antitumor efficacy of functional paclitaxel nanomicelles in treating resistant breast cancers by oral delivery. Biomaterials 32, 3285–3302.

Yee, S., 1997. In vitro permeability across Caco-2 cells (colonic) can predict in vivo (small intestinal) absorption in man—fact or myth. Pharmaceutical Research 14, 763–766.

Yeh, T.H., Hsu, L.W., Tseng, M.T., Lee, P.L., Sonjae, K., Ho, Y.C., Sung, H.W., 2011. Mechanism and consequence of chitosan-mediated reversible epithelial tight junction opening. Biomaterials 32, 6164–6173.

Zhang, Y., Li, X., Zhou, Y., Fan, Y., Wang, X., Huang, Y., Liu, Y., 2010. Cyclosporin A-loaded poly(ethylene glycol)-b-poly(D, L-lactic acid) micelles: preparation, in vitro and in vivo characterization and transport mechanism across the intestinal barrier. Molecular Pharmacology 7, 1169–1182.